Available online at www.sciencedirect.com
SCIENCE DIRECT®
Biomass and Bioenergy 28 (2005) 307–320
BIOMASS & BIOENERGY
www.elsevier.com/locate/biombioe

Straw combustion on slow-moving grates—a comparison of model predictions with experimental data

Søren K. Kær*

Institute of Energy Technology, Aalborg University, Pontoppidanstræde 101, DK-9220 Aalborg, Denmark

Received 31 July 2003; received in revised form 21 June 2004; accepted 9 August 2004
Available online 25 September 2004

Abstract

Combustion of straw in grate-based boilers is often associated with high emission levels and relatively poor fuel burnout. A numerical grate combustion model was developed to assist in improving the combustion performance of these boilers. The model is based on a one-dimensional "walking-column" approach and includes the energy equations for both the fuel and the gas accounting for heat transfer between the two phases. The model gives important insight into the combustion process and provides inlet conditions for a computational fluid dynamics analysis of the freeboard. The model predictions indicate the existence of two distinct combustion modes. Combustion air temperature and mass flow-rate are the two parameters determining the mode. There is a significant difference in reaction rates (ignition velocity) and temperature levels between the two modes. Model predictions were compared to measurements in terms of ignition velocity and temperatures for five different combinations of air mass flow and temperature. In general, the degree of correspondence with the experimental data is favorable. The largest difference between measurements and predictions occurs when the combustion mode changes. The applicability to full-scale is demonstrated by predictions made for an existing straw-fired boiler located in Denmark.

Keywords: Straw combustion; Grate-firing; Bed model; Model validation

1. Introduction

Internationally, there is an increasing interest in using biomass for power generation as a means to reduce the net emission of carbon dioxide to the atmosphere. Grate-fired boilers are commonly used for power generation from biofuels in the range from a few to about 100 MW thermal power. This is mainly due to a combination of relative simplicity, a high degree of fuel flexibility and reliability. In these boilers, the primary fuel conversion takes place on the grate. Therefore, it is of great interest to be able to predict the processes controlling important operational characteristics such as:

1. Release and oxidation of volatile gases.
2. Oxidations of the fuel char content.

*Tel.: +45-9635-9263; fax: +45-9815-1411.
E-mail address: skk@iet.aau.dk (S.K. Kær).

0961-9534/$ - see front matter © 2004 Elsevier Ltd. All rights reserved.
doi:10.1016/j.biombioe.2004.08.017

Nomenclature

A	cross-sectional area of computational cell in flow direction (m^2)
$A_{p,vol}$	particle surface area per unit volume (m^{-1})
A_V	pre-exponential factor of volatiles release (s^{-1})
C_p	specific heat capacity ($J\,kg^{-1}\,K^{-1}$)
d	diameter (m)
D_{AB}	diffusion coefficient ($m^2\,s^{-1}$)
h	heat transfer coefficient ($W\,m^{-2}\,K^{-1}$)
h_m	mass transfer coefficient ($m\,s^{-1}$)
H	enthalpy ($J\,kg^{-1}$)
k	thermal conductivity ($W\,m^{-1}\,K^{-1}$)
k_c	kinetic char oxidation rate ($kg\,m^{-2}atm\,s^{-1}$)
k_d	diffusion reaction rate ($kg\,m^{-2}atm\,s^{-1}$)
m	mass (kg)
Nu	Nusselt number (dimensionless)
Pr	Prandtl number (dimensionless)
p	pressure (pa)
r	radius (m)
R	universal gas constant ($J\,kmol^{-1}\,K^{-1}$)
R_i	gas constant ($J\,kg^{-1}\,K^{-1}$)
Re	Reynolds number (dimensionless)
S	source term (kg or $J\,m^{-3}\,s^{-1}$)
Sh	Sherwood number (dimensionless)
t	time (s)
T	temperature and activation temperature (K)
U	velocity (ms^{-1})
V	volatiles yield (kg)
V_f	final volatiles yield (kg)
W	molecular weight ($kg\,kmol^{-1}$)
x	location (m)
X	mass concentration ($kg\,m^{-3}$)
φ	mass fraction (dimensionless)
ρ	density ($kg\,m^{-3}$)
χ	CO_2 to CO molar ratio of char oxidation (dimensionless)

Subscripts

bed	parameter related to the bed material
C	carbon
Char	char content
CO	carbon monoxide
cyl	cylinder
Char→CO	char to CO reaction
CO→CO_2	CO to CO_2 reaction
devol	devolatilisation reaction
drying	drying of fuel
D	diameter
evap	evaporation
exchange	exchange between bed and gas
gas	gas phase
heat	heat equation
i	species index
mass	mass
O_2	oxygen
vap	vapor
vol→CO	volatiles to CO reaction
vol→CO_2	volatiles to CO_2 reaction
V	volatiles

3. The temperature fields of the fuel layer and the gas.
4. Species concentration fields, in this case; volatiles, O_2, CO, CO_2 and H_2O.
5. The release of inorganic compounds (mainly alkali salts) and environmentally harmful species.
6. Entrainment of particles from the bed surface.

This paper discusses an approach to predict items 1–4, however, the framework can be extended to include also items 5 and 6. Some of the processes 1–4 were addressed previously by other investigators using models of varying complexity [1–4]. Of these only the work by Van der Lans et al. [2] focused on straw combustion. This paper suggests a slightly different approach that, amongst other things, includes separate gas and fuel temperatures

that show good agreement with experimental data. Experimental investigations of the combustion properties of various biofuels in fixed beds were reported by Van der Lans et al. [5], DiBlasi et al. [6], Saastamoinen et al. [7], Horttainen et al. [8]. In this paper predictions are compared with the data of [5].

2. Model outline

A typical example of a grate-fired boiler including the fuel layer modeled is given in Fig. 1. Also indicated is the discretization of the bed employed in the numerical model. Conceptually, the model considers the fuel layer as a number of three-dimensional volumes. Each of these volumes is divided into horizontal slabs and a discrete node point located at the center of each slab represents the properties of the gas and the fuel. Fuel particles are assumed to be thermally thin, that is, the temperature as well as the composition of individual particles is uniform. This is a fairly good approximation for straws and grasses but not for typical wood chips. No attempt was made to model the macro-scale mixing caused by for example grate vibrations. Furthermore, the model does not account for the inhomogeneous character of the fuel and the potential formation of fuel lumps and flow channels through the bed.

Assuming the grate to be moving continuously at a constant velocity, U_{bed}, a simple relation between the position of the fuel on the grate, x, and its residence time, t, exists

$$t = \frac{x}{U_{\text{bed}}}(s) \Leftrightarrow x = U_{\text{bed}}\, t \quad \text{(m)}. \tag{1}$$

Fig. 2, which shows the heat transfer processes within the one-dimensional model illustrates this. At each new time step, or equivalently at each new x-position along the grate, the fuel composition and temperature from the previous is "transferred" to the new control volumes as initial conditions to simulate the motion of the fuel—a Lagrangian or "walking-column" approach.

3. Gas and bed governing equations

This section discusses the mass and energy conservation equations of the gas phase and the

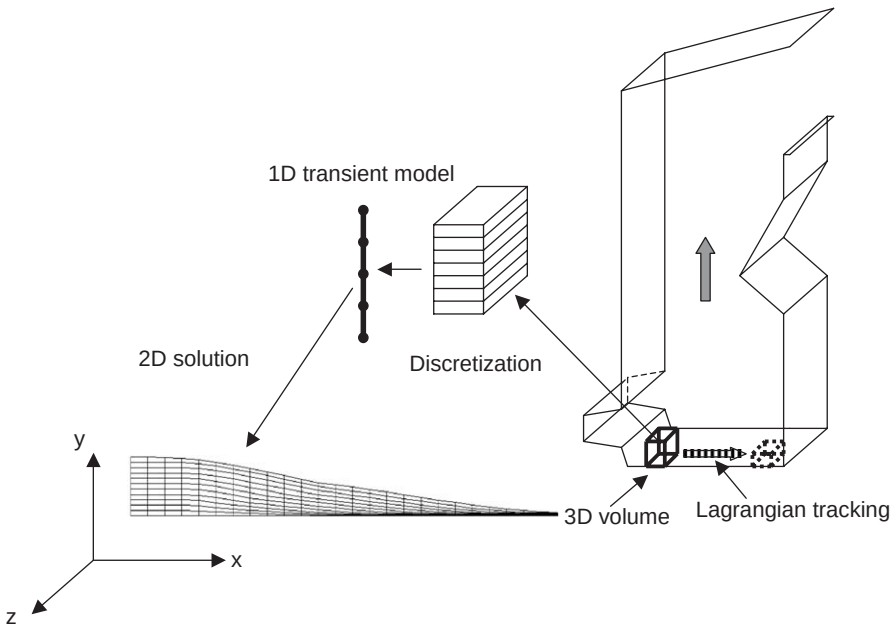

Fig. 1. Schematic of the fuel bed discretization used in the numerical model. Large arrows indicate overall flow direction.

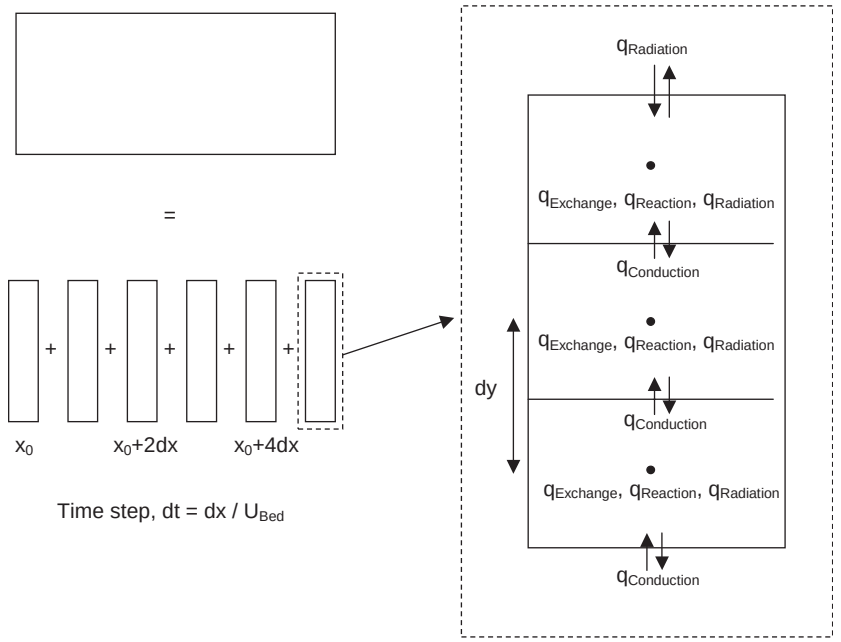

Fig. 2. Schematic of the transformation between time and space. The one-dimensional heat transfer model is also illustrated.

solid bed. Details about the source terms of the equations are given in the next section dealing with reactions and heat and mass transfer. The equations describing conservation of chemical species in the gas phase and the components of the bed will not be discussed in this paper.

3.1. Bed mass and energy conservation

Mass transport of the solid bed material is assumed to take place only in the direction along the grate as mentioned above. The continuity equation for the bed is given as

$$\frac{\partial(\rho_{\text{bed}})}{\partial t}+\frac{\partial(\rho_{\text{bed}}U_{\text{bed}})}{\partial x} = S_{\text{mass,drying}}+S_{\text{mass,devol}}+S_{\text{mass,char}} \times(\text{kg m}^{-3}\,\text{s}^{-1}), \quad (2)$$

where ρ_{bed} is the bed density and $S_{\text{mass},i}$ are source terms accounting for mass changes due to conversion of the bed.

The residence time of the fuel in a computational cell (given by the length of the cell in the x-direction and the fuel velocity) is too short for the heat transfer processes to reach a steady state in the vertical direction before it is transferred to the next x-position. Thus, the process is governed by the time-dependent one-dimensional heat conduction equation:

$$\frac{\partial(\rho_{\text{bed}}\,c_{p,\text{bed}}\,T_{\text{bed}})}{\partial t} = \frac{\partial}{\partial y}\left(k_{\text{bed}}\frac{\partial T_{\text{bed}}}{\partial y}\right)+S_{\text{heat,exchange}}+S_{\text{heat,drying}} + S_{\text{heat,char}} \quad (\text{W m}^{-3}), \quad (3)$$

where $c_{p,\text{bed}}$ is the specific heat, T_{bed} is the bed temperature and k_{bed} is the thermal conductivity of the fuel. The source terms, $S_{\text{heat},i}$ account for heat release from conversion of the bed and heat exchange with the gas phase. Heat transfer by convection of the bed in the x-direction is accounted for by the Lagrangian approach described above. Solid–solid radiative heat transfer in the bed is included using the Shuster–Schwarzschild approximation as discusssed in detail by Shin and Choi [4].

3.2. Gas phase mass and energy conservation

The gas is assumed to be transported in the vertical direction by convection driven by the air supplied from under the grate. The gas phase continuity equation is given by

$$\frac{\partial(\rho_{\text{gas}})}{\partial t}+\frac{\partial(\rho_{\text{gas}}U_{\text{gas}})}{\partial y} = -S_{\text{mass,drying}}-S_{\text{mass,devol}}-S_{\text{mass,char}} \quad (\text{kg m}^{-3}\,\text{s}^{-1}). \tag{4}$$

The gas velocity is predicted from the mean gas density using

$$U_{\text{gas}}=\frac{\dot{m}_{\text{gas}}}{\rho_{\text{gas}}A} \quad (\text{m s}^{-1}), \tag{5}$$

where $\dot{m}_{\text{gas}}$ is the vertical mass flow-rate of gas in the one-dimensional model and A is the cross-sectional area of the computational cell face. The density of each species i as a function of temperature is represented by the perfect gas law:

$$\rho_{\text{gas},i}=\frac{p}{R_i T_{\text{gas}}} \quad (\text{kg m}^{-3}), \tag{6}$$

where p is pressure, W_i molecular weight, R_i the gas constant and T_{gas} the gas temperature. Define the mass fraction of species i, φ_i (dimensionless) by

$$\varphi_i=\frac{m_i}{m_{\text{total,gas}}} \tag{7}$$

with m_i being the mass of species i and $m_{\text{total,gas}}$ the total mass of gas in the cell. The mean density of the gas mixture, ρ_{gas}, is

$$\rho_{\text{gas}}=\left(\sum_{i=1}^{i=n}\frac{\varphi_i}{\rho_{\text{gas},i}}\right)^{-1} \quad (\text{kg m}^{-3}). \tag{8}$$

The source terms $S_{\text{mass},i}$ account for mass transfer resulting from reactions in the bed.

The gas phase thermal heat conduction is negligible compared to convection as the Péclet number is of the order of 100. The energy equation is thus given by

$$\frac{\partial(\rho_{\text{gas}}c_{p,\text{gas}}T_{\text{gas}})}{\partial t}+\frac{\partial}{\partial y}(\rho_{\text{gas}}U_{\text{gas}}c_{p,\text{gas}}T_{\text{gas}}) = -S_{\text{heat,exchange}}+S_{\text{heat,vol}}+S_{\text{heat,CO}} \quad (\text{W m}^{-3}), \tag{9}$$

where $c_{\text{p,gas}}$ is the gas specific heat and $S_{\text{heat},i}$ are source terms accounting for heat exchange with the bed and heat release from reactions in the gas phase.

The numerical solution of Eqs. (2)–(4) and (9) is discussed by Patankar [9], amongst many others, and no further details will be included here.

3.3. Heat exchange between the phases

The convective exchange of heat between the fuel bed and the gas is included through the source terms of the energy equations (Eqs. (3) and (9)). In the present case, a heat transfer correlation for a circular cylinder (approximate shape of straw) in cross-flow was adopted [10].

$$\overline{Nu}_{\text{cyl}}=\frac{\bar{h}d_{\text{cyl}}}{k_{\text{gas}}} = 0.3+\frac{0.62Re_{\text{D}}^{1/2}Pr^{1/3}}{[1+(0.4/Pr)^{2/3}]^{1/4}}\times\left[1+\left(\frac{Re_{\text{D}}}{282,000}\right)^{5/8}\right], \tag{10}$$

where Nu_{cyl} is the average Nusselt number (dimensionless), h the average convective heat transfer coefficient, d_{cyl} the cylinder diameter, k_{gas} the thermal conductivity of the gas, Re_{D} the cylinder Reynolds number and Pr is the Prandtl number. The rate of convective heat exchange is given by

$$S_{\text{heat,exchange}}=\overline{h}A_{\text{p,vol}}(T_{\text{gas}}-T_{\text{bed}}) \quad (\text{W m}^{-3}). \tag{11}$$

The total particle surface area per unit volume of the fuel layer, $A_{\text{p,vol}}$, is calculated assuming the fuel particles are hollow cylinders. The outer surface area to volume ratio is given by

$$A_{\text{p,vol}}=\frac{2r_{\text{outer}}}{(r_{\text{outer}}^2-r_{\text{inner}}^2)} \quad (\text{m}^{-1}). \tag{12}$$

4. Chemical conversion of the bed

4.1. Evaporation of moisture

The drying process is important as the evaporation of water influences both the temperature fields and the burnout time. Below the boiling point, the evaporation rate is calculated based on a mass transfer correlation. At the boiling point, the evaporation rate is controlled by the heat transfer rate to the fuel. Due to the assumption of thermally thin particles, all the water has to evaporate before the onset of devolatilization. For straws and grasses, this is a reasonable approximation. For typical wood chips significant internal temperature and concentration gradients may occur due to finite heat and mass transfer rates. The water vapor mass flux leaving the fuel due to mass transfer is given by

$$S_{\text{mass,drying}} = \bar{h}_{\text{m}} A_{\text{p,vol}} (X_{\text{gas}} - X_{\text{surface}}) \quad (\text{kg m}^{-3}\,\text{s}^{-1}), \tag{13}$$

where the mean mass transfer coefficient is approximated from a Sherwood number correlation (dimensionless) for a cylinder and X is the mass concentration in the gas and at the particle surface. Using the analogy between heat and mass transfer Eq. (10) can be used to estimate the mass transfer coefficient

$$\overline{Sh}_{\text{cyl}} = \frac{\overline{h_{\text{m}}} d_{\text{cyl}}}{D_{\text{AB}}}. \tag{14}$$

The diffusivity, D_{AB}, of the vaporizing species in the gas mixture, is approximated by the binary diffusivity of the species in air using the method suggested by Wilke and Lee [11]. The vapor mass concentration at the particle surface is calculated from the vapor pressure at the surface of the fuel particles using a slightly simplified form of the Clausius–Clapeyron equation that neglects the condensed phase volume and expresses the gas phase volume using the perfect gas law [12].

$$\frac{\text{d}\,\text{In}\,(p_{\text{vap}})}{\text{d}T} = \frac{H_{\text{evap}}}{RT^2} \quad (\text{K}^{-1}). \tag{15}$$

The resulting source term in the bed energy equations is

$$S_{\text{heat,drying}} = S_{\text{mass,drying}} H_{\text{evap}} \quad (\text{W m}^{-3}), \tag{16}$$

where H_{evap} is the heat of evaporation of the evaporating species.

4.2. Volatiles release and combustion

The volatiles release rate is modeled by a simple first-order Arrhenius expression with a pre-exponential factor of $10^6\,\text{s}^{-1}$ and an activation temperature of 9000 K [13]:

$$k_V = A_{\text{V}} \exp\left(-\frac{T_{\text{V}}}{T_{\text{bed}}}\right) \quad (\text{s}^{-1}). \tag{17}$$

The resulting mass source in the gas and bed continuity equations is

$$S_{\text{mass,devol}} = -\rho_{\text{bed}} k_{\text{V}} (V_{\text{f}} - V) \quad (\text{kg}_{\text{V}}\,\text{m}^{-3}\,\text{s}^{-1}), \tag{18}$$

where V and V_{f} are the mass of volatiles released from unit mass of raw fuel and the final volatiles yield, respectively. The amount and composition of the volatiles is prescribed in advance with this model, although in reality they depend on factors such as heating rate and maximum temperature. More complex models that take these factors into account exist; however, they require a larger amount of experimentally determined data, which are not always readily available. The volatiles yield under typical combustion conditions exceeds that given by a standard ASTM proximate analysis. In the present case, volatiles yields measured at typical combustion temperatures and heating rates were used. The composition of the volatiles was estimated based on proximate and ultimate analyses of the fuel, by subtracting the amount of C that is tied up in fixed char from that given by the ultimate analysis. For a typical wheat straw, the average pseudo volatile gas composition is $CH_{1.6}O_{0.8}$. This is based on the ultimate analysis presented in Table 1.

The combustion of volatiles in the gas phase is modeled as either a full oxidation to CO_2 or a partial oxidation to CO. At present, an equal mass of CO_2 and CO is assumed to evolve which is based on values measured by Van der

Table 1
The ultimate (major species) and proximate analyses used in the predictions

Ultimate analysis	wt%	Proximate analysis (dry)	wt%
C	44.6	Ash	5
H	5.9	Fixed carbon	10
O	49.5	Volatiles	85
		LHV as received	14.9 MJ kg^{-1}

Lans et al. [5] during fixed bed combustion of straw. The reactions are assumed infinitely fast in the presence of oxygen. The heat released in the gas phase due to volatiles oxidation is given as

$$S_{\text{heat,vol}} = -\frac{\mathrm{d}m_{\text{Vol}\to\text{CO}}}{\mathrm{d}t} H_{\text{Vol}\to\text{CO}} - \frac{\mathrm{d}m_{\text{Vol}\to\text{CO}_2}}{\mathrm{d}t} H_{\text{Vol}\to\text{CO}_2} \quad (\text{W m}^{-3}), \quad (19)$$

where the first-term on the right-hand side expresses the mass of volatiles oxidized to CO per unit volume per second times the heat released from the reaction. The second-term is similar only for the full oxidation of the volatiles.

4.3. Char oxidation

Char is assumed to be either fully or partially oxidized at the particle surface forming CO_2 or CO. In comparison with experimental data, the ratio was fixed based on the measurements. In full-scale simulation, the temperature dependence of the CO_2 to CO ratio, χ, was based on an Arrhenius expression with a pre-exponential factor of 33 kmol/kmol and an activation temperature of 4700 K [14]. Defining the following ratio: $\varphi = (\chi + 1\chi + 0.5)$; $1 \leqslant \varphi \leqslant 2$ allows the C–O_2 reaction to be expressed as

$$C + \frac{1}{\varphi}\mathrm{O_2} \to \left(2 - \frac{2}{\varphi}\right)\mathrm{CO} + \left(\frac{2}{\varphi} - 1\right)\mathrm{CO_2}. \quad (20)$$

The rate of char oxidation is modeled as a combination of the kinetic reaction rate, k_c, and the rate of oxygen diffusion to the surface, k_d. The total oxidation rate based on the combined kinetic and diffusion rates is given by

$$S_{\text{mass,char}} = -\frac{\varphi}{k_d^{-1} + k_c^{-1}} p_{\mathrm{O_2}} A_{\text{p,vol}} \quad (\text{kg m}^{-3}\ \text{s}^{-1}). \quad (21)$$

At lower temperatures, kinetics control the reaction rate, whereas oxygen diffusion is the limiting term at temperatures exceeding about 800 °C in the case of a typical 5 mm diameter straw particle.

The heat released by oxidation of char to CO is added to the bed energy equation whereas heat released by subsequent oxidation of CO to CO_2 in the gas phase is added in the gas energy equation. For the bed this gives

$$S_{\text{heat,char}} = -S_{\text{mass,char}} H_{\text{char}\to\text{CO}} \quad (\text{W m}^{-3}), \quad (22)$$

where $H_{\text{char}\to\text{CO}}$ is the heat released from oxidation of unit mass of char to CO. For the gas phase the source term is

$$S_{\text{heat,CO}} = -S_{\text{mass,char}} \frac{W_{\text{CO}}}{W_{\text{C}}} \left(\frac{\varphi}{2} - 1\right) H_{\text{CO}\to\text{CO}_2} \quad (\text{W m}^{-3}), \quad (23)$$

where W_{CO} and W_{C} are the molecular weights of CO and C, respectively. $H_{\text{CO}\to\text{CO}_2}$ is the heat released from oxidation of unit mass of CO to CO_2.

5. Model results

In this section model results are presented for two cases. The first is a comparison of model predictions with experimental results from fixed bed combustion of straw [5]. The second is a simulation of the process in a full-scale grate-fired boiler.

5.1. Batch combustion of straw

The combustion of a batch of straw was studied by Van der Lans et al. [5] in a cylindrical furnace, among other things, to simulate the process in the fuel bed of grate-fired boilers. The experimental setup used is illustrated in Fig. 3. The bed temperature as a function of time was measured at the positions (vertical spacing 15 cm) indicated in Fig. 3 as well as the weight of the bed and the

exit gas composition (O_2, CO_2, CO, NO_X, SO_X, C_XH_Y, H_2O and NH_3). Experiments were made using air mass flow-rates ranging from 0.072 to 0.18 $kg\,m^{-2}\,s^{-1}$ and temperatures of 20 and 150 °C. This allows comparison to be carried out covering a range of important operational parameters. A Danish wheat straw cut to an average length of 20 mm was used in the experiments. In the predictions, moisture content of 5 wt% at the onset of the measurements was assumed. The bed bulk density is reported to be 80–90 $kg\,m^{-3}$ and in the predictions the average value of 85 $kg\,m^{-3}$ was used. For a detailed description of the experimental procedure please refer to [5].

5.2. Combustion modes

The numerical predictions indicated that two combustion modes with significantly different characteristics exist. An understanding of the combustion mode or pattern is important to the interpretation of the results. Throughout this discussion it is assumed that the top of the bed is heated by radiation from the furnace. At relatively low air mass fluxes and temperatures, combustion proceeds in two distinct steps (this will be called mode 1). In the first, a reaction front is moving from the top of the bed towards the bottom. During this stage release of moisture and volatiles are the dominant processes. In the second region, which is initiated when the first front reaches the grate, a reaction front is moving upwards and the remaining char burns out. This is illustrated schematically in Fig. 4a. At higher air mass fluxes and temperatures, the combustion mode changes as the relatively high mass flux of warm air heats up the lower portion of the bed causing drying, volatiles release and char oxidation to initiate from below (this will be called mode 2). The velocity of the devolatilization front is significantly faster in this mode because the hot products from volatiles combustion and possibly char oxidation heat up the upper portion of the fuel layer as they leave the bed. Fig. 4b illustrates this overall reaction pattern.

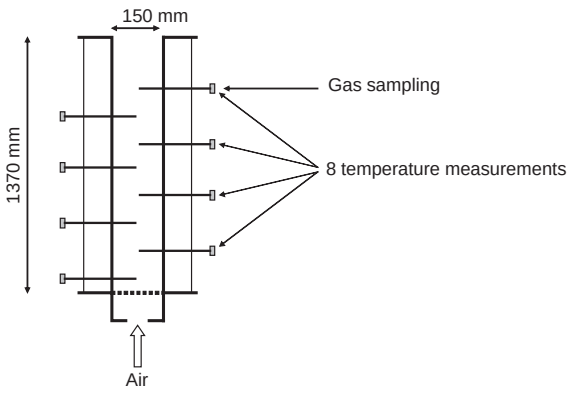

Fig. 3. The experimental setup used to study batch combustion of straw.

The existence of two combustion modes as described above were also presented in [15] based on a combination of theoretical considerations and experimental data. It is clear that the combustion air temperature is too low to cause char oxidation to initiate at the grate. In the full-scale furnace it is suggested by Thunman [15], that burning particles are trapped on the grate causing ignition of the fuel. In the numerical model,

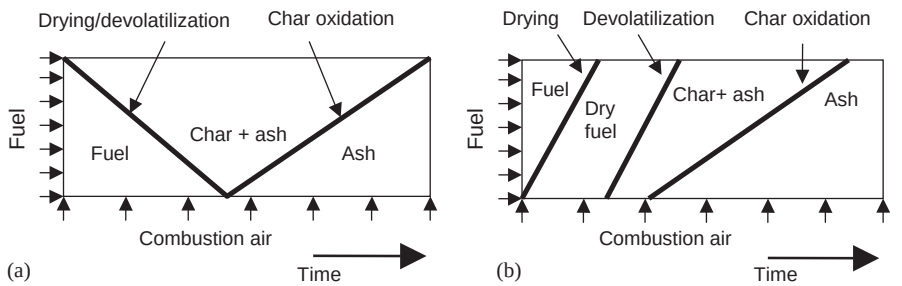

Fig. 4. Schematic illustration of the two suggested combustion modes.

ignition results from the assumption of infinitely fast volatiles combustion. Volatiles are released at the grate when the temperature reaches the devolatilization temperature of biomass (around 150–200 °C) due to heating by the combustion air. Initially, the released volatiles react with the combustion air supplying the heat required to initiate char oxidation. From this point, the upward moving front sustains itself primarily by char oxidation. Although this ignition process is not physically realistic the resulting combustion pattern seems plausible given the findings reported by Thunman [15].

5.3. Overall fuel conversion

The time it takes for the first reaction front to reach the grate and the time it takes for the remaining char to burn can be used as overall parameters for comparison between the model and the experiment. Monitoring the weight of the fuel bed identifies the two regions. The bed weight as a function of time predicted using the condition given above is shown in Fig. 5. The devolatilization process (the part with a steep slope) was predicted to last about 32–34 min, which is in very good correspondence with the measured duration of 30–35 min [5]. For the char burnout phase, the values are more difficult to estimate since the change in mass is slower. The predicted as well as the measured durations are estimated to be approximately 25–30 min.

The ignition velocity is a characteristic parameter that expresses the velocity at which the devolatilization front travels towards the grate, i.e., bed height divided by total devolatilization time. Using this parameter, comparison is made for all air mass fluxes and temperatures in Fig. 6. The predicted variation of the ignition velocity as a function of air mass flux at an air temperature of 20 °C is in close agreement with measured values. The reproducibility of the measured ignition velocity was within ±5% of the average [5]. At an air temperature of 150 °C, predicted ignition velocities are lower than corresponding experimental data, especially at the low air mass flux of $0.12\,kg\,m^{-2}\,s^{-1}$. At the high air temperatures, the model predicts an increase in ignition velocity with air mass flux, whereas the measurements indicate an almost constant value of around 8 cm/min.

It is believed, that the difference between measurements and predictions at an air temperature of 150 °C is closely related to a beginning change in the combustion modes, i.e., going from the pattern illustrated in Fig. 4a to that shown in Fig. 4b. To illustrate this process, the predicted ignition velocity (running average) as a function of time during devolatilization is shown in Fig. 7 for air mass fluxes of 0.12 and $0.18\,kg\,m^{-2}\,s^{-1}$ and an air temperature of 150 °C. The ignition velocity exhibits a strong increase as devolatilization and volatiles combustion initiates and subsequently the increasing tendency continues but at a much slower rate. As the ignition velocity starts

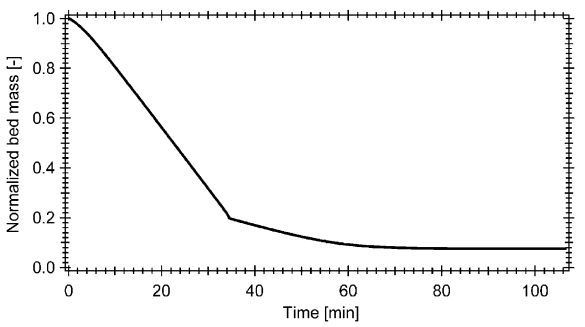

Fig. 5. Normalized bed mass as a function of reaction time. The airflow rate in this case is $0.18\,kg\,m^{-2}\,s^{-1}$ and the temperature is 20 °C.

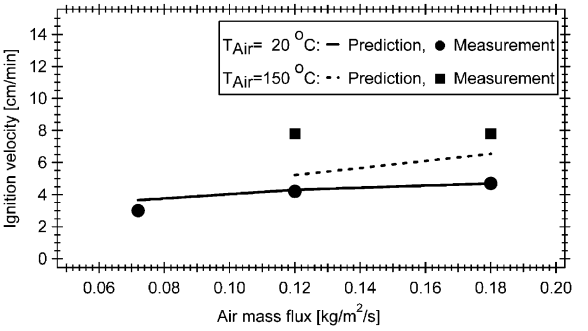

Fig. 6. Predicted and measured ignition velocities as a function of air mass flux at air temperature of 20 and 150 °C, respectively.

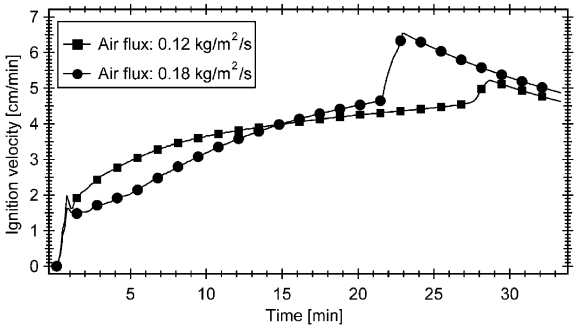

Fig. 7. Predicted ignition velocity (running average) as a function of time at an air temperature of 150 °C and air mass fluxes of 0.12 and 0.18 $kgm^{-2}s^{-1}$, respectively.

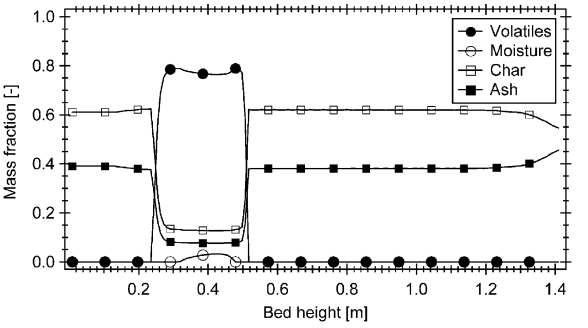

Fig. 8. Fuel bed composition 22 min after ignition showing unreacted fuel only in the middle of the fuel layer suggesting that devolatilization fronts were moving both from the bottom up and from the top down.

decreasing, devolatilization has ended and char oxidation begun. At lower temperatures, the ignition velocity approaches a constant value where the heat release and heat transfer mechanisms are in equilibrium. In Fig. 7, the ignition velocity increases abruptly after 28 min in the low air mass flux case, which can be ascribed to a change in the combustion mode. At this point, the heating of the bed from below by the air has caused the bed temperature to reach a level where devolatilization initiates. Consequently, the devolatilization front now travels upwards and, as discussed previously, this mode favors a higher ignition velocity. This is further supported by the fact that the sharp increase occurs after only 20 min at an air mass flux of 0.18 $kg\,m^{-2}\,s^{-1}$ due to the higher heating rate of the lower part of the bed. Moreover, it can be seen directly from the bed composition as a function of vertical position.

In Fig. 8 the composition is shown as a function of bed height 22 min after ignition. As seen from the mass fraction of volatiles, devolatilization has initially taken place from the top of the bed (mode 1) and down to a position approximately 0.5 m above the grate. Subsequently, another devolatilization front has started to move upwards (mode 2) from the grate and reached a position approximately 0.2 m above the grate. The strong dependence of the predicted ignition velocity on the combustion mode and the complex nature of the ignition process when going from modes 1 to 2 make it extremely difficult to accurately predict the ignition velocity in this regime. Auto-ignition of

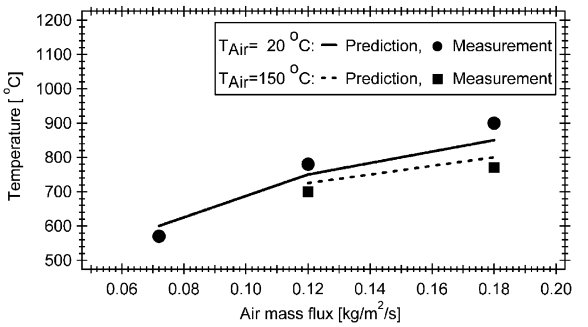

Fig. 9. Comparison of predicted and measured temperatures in the downward moving front as a function of air mass flux at air temperatures of 20 and 150 °C, respectively.

the fuel was reported by Van der Lans et al. [5] at an air temperature of 200 °C, which further supports the idea of a beginning change in combustion pattern.

5.4. Temperatures vs. air mass flux

The peak temperatures measured as the downward and upward moving reaction fronts passed the thermocouples were almost independent of the vertical position of the thermocouple in the bed [5]. The ability of the model to predict these temperature levels as a function of air mass flux and temperature provides a good measure of the accuracy of the temperatures calculated.

Fig. 9 presents a comparison between measured and predicted temperatures for both air

temperatures and all air mass fluxes used. There is good correspondence between predicted and measured combustion temperatures in the downward moving front within the range of air mass fluxes and temperatures investigated. The predicted dependence of the temperature on air temperature as well as air mass flux is too weak. Still, the right trends are captured. The temperature increase with air mass flux is due to an increasing amount of fuel burning in the bed as the air-to-fuel ratio increases. Increasing the air mass flux to an air-to-fuel ratio larger than the stoichiometric value would cause the temperature to decrease. The decrease of the temperature with increasing air temperature is interesting. It is related to the increasing velocity of the devolatilization front at higher air temperatures, which results in a decreasing air-to-fuel ratio in the reaction front. This indicates an ability to control the temperature in the bed that may have important implication to the operation of the boiler.

The temperatures in the upward moving front are presented in Fig. 10, as a function of air mass flux and temperature. The predicted temperatures are too high, especially at low air mass fluxes and temperatures, whereas very good agreement is found at the high air mass flux at both temperatures. As for the temperature in the downward moving front, there seems to be a tendency for the model to predict a too weak dependence of the temperature on air mass flux. This can possibly be related to the model used for convective heat transfer between the gas and the fuel underestimating the change in heat transfer rate with air mass flux. The fact that the temperature in the upward moving front is lower at high air temperatures is a result of the lower temperature of the fuel after devolatilization, cf. Fig. 9.

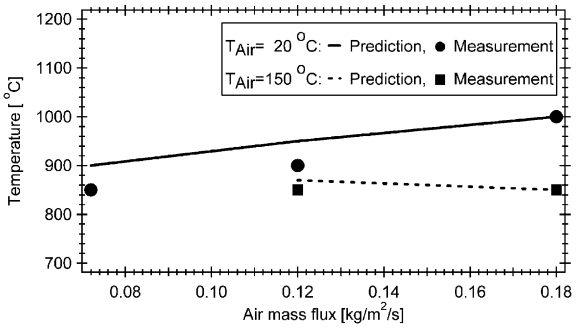

Fig. 10. Comparison of predicted and measured temperatures in the upward moving front as a function of air mass flux at air temperatures of 20 and 150 °C, respectively.

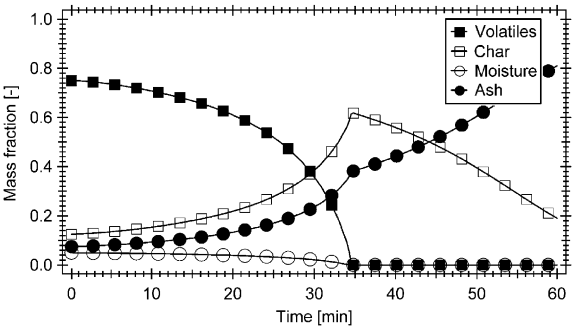

Fig. 11. Average composition of the fuel layer as a function of time. The devolatilization zone extends the first 30 min followed by char oxidation.

5.5. Bed compositions vs. time

The average composition of the bed, as a whole, during the first hour of combustion is illustrated in Fig. 11 for the case with an air mass flux of $0.12\,kg\,m^{-2}\,s^{-1}$ and a temperature of 20 °C. The rate of devolatilization is seen to accelerate, especially towards the end of the process. Char oxidation, on the other hand, progresses at an almost constant rate indicating the process is limited by oxygen diffusion.

6. Full-scale model demonstration

To demonstrate the applicability of the model to full-scale boilers a prediction was made for a Danish straw-fired plant. The boiler is an auger feed system where the fuel enters the furnace at one side and the ash leaves enters the system at the opposite side of the grate. Frequent (approximately every 150 s) vibrations (2–3 s duration) of the slightly tilted grate transport the fuel across the grate. The process data used are summarized in Fig. 12.

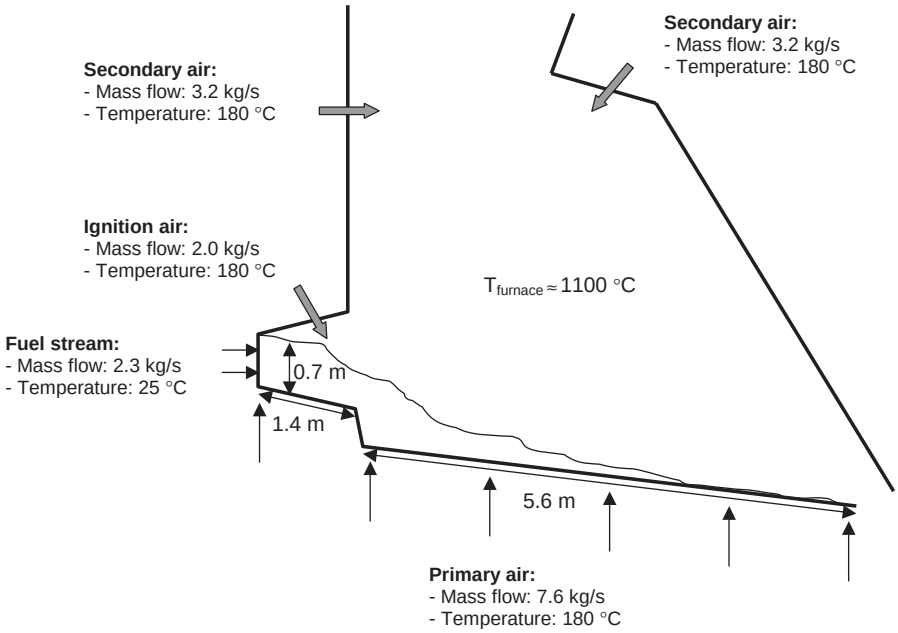

Fig. 12. Schematic illustration of the lower section of a grate fired boiler giving the operating condition used in the demonstration of the bed model to a full-scale boiler.

6.1. Model configuration

A grid containing 250 points in the vertical direction was used and the residence time of the fuel on the grate was resolved by 1000 time steps. Approximate 5–10 min were used in order to complete the calculation on a PC. The computational grid was adapted in each time step to the height of the fuel bed. An overall straw bed density of 60 kgm^{-3} was used which is representative for the straw as it enters the furnace. No primary air is introduced in the so-called devolatilization zone of the grate, which extends the first 1.4 m of the bed, cf. Fig. 12. In this zone there is a strong interaction with the ignition air injected from nozzles located above the fuel feeder port (see Fig. 12). The model cannot predict the penetration of these air jets into the fuel layer. Neglecting the ignition air in the model would cause devolatilization to initiate too far from the fuel feeding port. To obtain more realistic model predictions, primary air has also been added in the devolatilization zone.

6.2. The overall bed combustion pattern

Fig. 13, showing the mass fraction of char in the bed predicted by the model, illustrates the combustion process on the grate. Only the first 5 m is shown as char burnout is almost complete at that point. The strong increase in char mass fraction close to the fuel feeding port indicates the onset of devolatilization. The process is initiated by flame radiation heating and moves from the top and downwards. This reaction pattern agrees with that expected from the location of the ignition air nozzles. The devolatilization front reaches the grate at a distance of about 1.5 m from the fuel feeding port. At that point, the char oxidation front starts moving from the bottom up. Compared with the devolatilization front, the char oxidation front is much wider due to oxygen diffusion being the limiting reaction process.

Fig. 14 illustrates the predicted bed temperature field (Celsius) in the first 5 m of the fuel layer. The reaction of volatiles in the fuel layer raises the temperature of the char left in the devolatilized

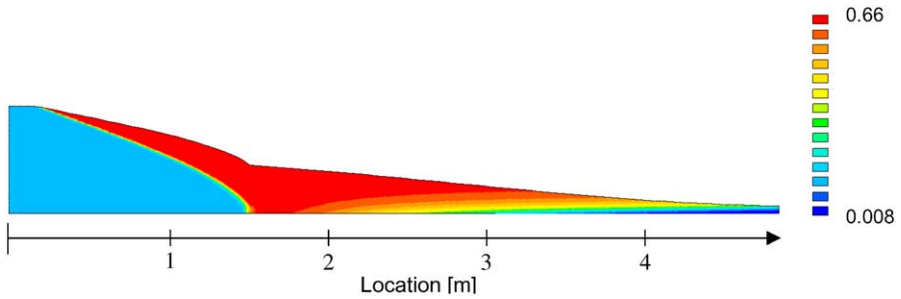

Fig. 13. Two-dimensional illustration of fuel bed char content. Only the first 5 m of the grate is included, as char burnout has almost completed at that point.

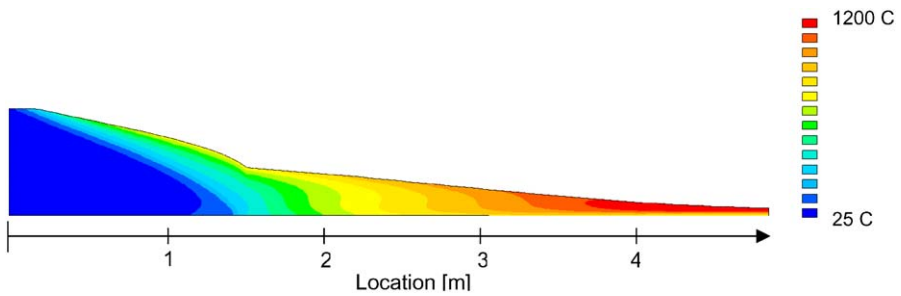

Fig. 14. Two-dimensional illustration of fuel layer temperature. Again only the first 5 m of the grate is included.

region to approximately 600–700 °C. The temperature gradient in the vertical direction is much weaker than suggested by the narrow devolatilization front. This is due to the finite rate of heat transfer from the gas to the bed. In the char oxidation zone, the temperature increases further along the grate as the heat released by oxidation of char to CO accumulates in the bed. The maximum bed temperature is approximately 1200 °C at the location of complete char burnout.

7. Conclusions

One-dimensional "walking-column" model was developed to investigate the combustion behavior of straw on a vibrating grate. The model considers the fuel and the gas as two separate phases and accounts for the heat transfer between them. When compared with batch combustion experiments reported by Van der Lans et al. [5] very good agreement was found over a range of air temperatures and mass flows. The predictions indicated that two combustion patterns exist with distinct differences. The first mode is characterized by a devolatilization front that moves downwards followed by an upward moving char oxidation front. In the second mode devolatilization and char oxidation initiates at the grate and moves upwards. The ignition velocity is significantly faster in the second mode and the gas temperature is lower. The existence of two combustion modes is supported by the findings of Thunman [15]. Still, more experiments with straw and a more detailed model for volatiles oxidation kinetics is required to draw any final conclusions regarding this issue. A full-scale straw fired boiler was modeled to demonstrate the application of the model to an existing boiler. The combustion pattern for this system was of the first mode type with distinct devolatilization and char oxidation regions.

Acknowledgements

The Danish Energy Research Program and Babcock&Wilcox Vølund Aps, Denmark supported part of this work. Robert van der Lans from the CHEC research group at the Danish Technical University is thanked for providing the experimental data used for model validation.

References

[1] Radulovic P, Ghani M, Smoot LD. An improved model for fixed bed coal combustion and gasification. Fuel 1995;74(4):582–94.
[2] van der Lans RP, Pedersen LT, Jensen A, Glarborg P, Dam-Johansen K. Modelling and experiments of straw combustion in a grate furnace. Biomass & Bioenergy 2000;19:199–208.
[3] Larfeldt J, Tao L, Berge N. Development of an engineering tool for design and optimization of biomass combustion in grate-fired boilers. In: Proceedings of the fifth European conference on industrial furnaces and boilers, Portugal: 2000.
[4] Shin D, Choi S. The combustion of simulated waste particles in a fixed bed. Combustion and Flame 2000;121(1–2):167–80.
[5] van der Lans RP. Straw combustion in grate furnace—fixed bed experiments. CHEC report 9823, Department of Chemical Engineering, Technical University of Denmark: 1998.
[6] DiBlasi C, Portoricco G, Borrelli M, Branca C. Oxidative degradation and ignition of loose-packed straw beds. Fuel 1999;78:1591–8.
[7] Saastamoinen JJ, Taipale R, Horttanainen M, Sarkomaa P. Propagation of the ignition front in beds of wood particles. Combustion and Flame 2000;123:214–26.
[8] Horttainen MVA, Saastamoinen JJ, Sarkomaa PJ. Ignition and flame spread in fixed beds of wood particles. In: Proceedings of the fifth European conference on industrial furnaces and boilers, Portugal: 2000.
[9] Patankar SV. Numerical heat transfer and fluid flow, Series in Computational methods in mechanics and thermal sciences. Washington, DC: Hemisphere Publishing Corp.; 1980.
[10] Mills A F. Heat and mass transfer. 1st ed. Homewood, IL: Irwin; 1995.
[11] Reid RC, Prausnitz JM, Poling BE. The properties of gases and liquids, 4th ed. New York: McGraw-Hill; 1987.
[12] Denbigh K. The principles of chemical equilibrium, 4th ed. Cambridge: Cambridge University Press; 1987.
[13] Bech NL, Wolff L, Germann L. Mathematical modeling of straw bale combustion in cigar burners. Energy & Fuels 1996;10(2):276–83.
[14] van del Lans RP. EFP2000 joint project report, Department of Chemical Engineering, Danish Technical University, Denmark: 2001.
[15] Thunman H, Leckner B. Ignition and propagation of a reaction front in cross-current bed combustion of wet biofuels. Fuel 2001;80:473–81.